ac electric and magnetic responses of nonconnected Aharonov-Bohm rings

R. Deblock,[1] Y. Noat,[2] B. Reulet,[1] H. Bouchiat,[1] and D. Mailly[3]
[1]*Laboratoire de Physique des Solides, Associé au CNRS, Bâtiment 510, Université Paris-Sud, 91405, Orsay, France*
[2]*Kamerlingh Onnes Laboratory, Niels Bohrweg 5, Leiden, Netherlands*
[3]*CNRS Laboratoire de Microstructure et Microélectronique, 196 Avenue Ravera, 92220, Bagneux, France*
(Received 22 June 2001; revised manuscript received 12 September 2001; published 7 January 2002)

The signature of phase coherence on the electric and magnetic response of 10^5 nonconnected Aharonov-Bohm rings is measured by a resonant method at 350 MHz between 20 mK and 500 mK. The rings are etched in a GaAs-$Al_xGa_{1-x}As$ heterojunction. Both quantities exhibit an oscillating behavior with a periodicity consistent with half a flux quantum $\Phi_0/2=h/2e$ in a ring. We find that electric screening is enhanced when time-reversal symmetry is broken by magnetic field, leading to a *positive* magnetopolarizability, in agreement with theoretical predictions for isolated rings at finite frequency. Temperature and electronic-density dependences are investigated. The dissipative part of the electric response, the electric absorption, is also measured and leads to a *negative* magnetoconductance. The magnetic orbital response of the very same rings is also investigated. It is consistent with *diamagnetic* persistent currents of 0.25 nA. This magnetic response is an order of magnitude smaller than the electric one, in qualitative agreement with theoretical expectations.

DOI: 10.1103/PhysRevB.65.075301 PACS number(s): 73.20.Fz, 73.23.Ra

I. INTRODUCTION

At mesoscopic scale and at low temperature, electrons in metallic samples keep their phase coherence on a length L_Φ, which is bigger than the sample size. Transport and thermodynamic properties of the system are then sensitive to interference between electronic wave functions and present spectacular signatures of this phase coherence. To study these effects the ring geometry is especially suitable. Indeed in the presence of a magnetic flux Φ through the ring the periodic boundary conditions for electronic wave functions acquire a phase factor $2\pi\Phi/\Phi_0$ with $\Phi_0=h/e$ the flux quantum.[1] As a result, the magnetoconductance of a phase-coherent ring exhibits quantum oscillations the periodicity of which corresponds to one flux quantum through the area of the sample.[2] The phase of the first harmonics of these oscillations is sample specific so that these harmonics do not survive ensemble average. In contrast the second harmonics have a contribution that resists this averaging. This results from the interference between time-reversed paths around the ring (weak localization contribution). These $\Phi_0/2$ periodic oscillations were observed in transport measurements on long cylinders or connected arrays of rings.[3,4] Their sign corresponds to a positive magnetoconductance in zero field. In the case of singly connected geometries, such as full disks, the signature of weak localization consists in a single peak of positive magnetoconductance the width of which corresponds to $\phi_0/2$ through the sample.[5,6]

Magnetotransport experiments on connected systems constitute a very sensitive and powerful probe for the investigation of sample specific signatures of quantum transport. However, because of strong coupling between the system and the measuring device, quantum corrections represent a small fraction of the conductance (of the order of $1/g$, where g is the dimensionless conductance expressed in e^2/h units) that is still dominated by the classical Drude response in the diffusive regime $g\gg 1$. There exists a number of experiments that can address some of the electronic properties of mesoscopic samples without coupling to macroscopic wires. This is the case of ac conductance experiments where Aharonov-Bohm rings are coupled to an electromagnetic field. In contrast with the connected case, the response of an isolated system can be dominated by quantum effects. Moreover, the quasidiscrete nature of the energy spectrum and the sensitivity to the statistical ensemble (canonical or grand canonical) are new features of isolated mesoscopic systems. In particular, it has been emphasized that the average absorbtion of isolated mesoscopic systems is determined by the energy level statistics and its sensitivity to time-reversal symmetry breaking by a magnetic field.

The first experiments done in this spirit were performed by coupling an array of disconnected GaAs/$Ga_xAl_{1-x}As$ rings to a strip-line superconducting resonator.[7] In such a geometry the rings experience both ac magnetic and electric fields. The magnetic response of the rings, i.e., their orbital magnetism, is directly related to persistent currents in the zero-frequency limit.[8–13] On the other hand, the electric response of the isolated metallic sample is related to the screening of the electric field inside the metal. The induced charge displacement is at the origin of the polarizability α, defined as the ratio between the induced electric dipole $\mathbf{d}$ and the applied electric field $\mathbf{E}$ ($\mathbf{d}=\alpha\mathbf{E}$). The polarizability is known to be essentially determined by the geometry of the sample with correction of the order of λ_s/L, with λ_s the screening length and L the typical size of the system.[14] It has been recently predicted that this quantity is sensitive to phase coherence around the ring[15–17] and is thus expected to present flux oscillations. The electric contribution can be, in the particular case of GaAs rings, of the same order of magnitude as the magnetic response.[18]

To be able to distinguish between the two types of response we have designed a superconducting LC resonator in which the capacitive part and inductive part are physically separated. In this paper we present measurements of both the magnetic and electric responses of Aharonov-Bohm rings. Note that these experiments are done on the very same array

TABLE I. Characteristics of the rings after illumination.

Nominal density n		3×10^{11} cm^{-2}
Thomas Fermi screening length λ_s (Ref. 21)	$\lambda_s=(\pi/2)4\pi\epsilon_0\epsilon_r\hbar^2/(me^2)$	16 nm
Perimeter L		5.2 μm
Etched width		0.5 μm
Effective width W (Ref. 22)		0.2 μm
Phase coherence length L_Φ (Ref. 22)		6.5 μm
Mean free path l_e (Ref. 22)		3 μm
Diffusion coefficient D	$D=v_F l_e/2$	0.335 m^2 s^{-1}
Mean level spacing Δ	$\Delta=h^2/(2\pi mWL)$	80 mK or 1.66 GHz
Thouless energy E_c	$E_c=hD/L^2$	450 mK or 9.34 GHz
Dimensionless conductance g	$g=E_c/\Delta$	5.6

of rings for both types of response, giving us the opportunity to compare them. A preliminary account of the measurement of the electric response was given in Ref. 19.

The paper is organized in the following way. Section II gives a detailed presentation of the sample, an array of Aharonov-Bohm rings, and the resonating technique used to measure the magnetic and electric response. Results on the nondissipative part of the flux-dependent electric response are presented in Sec. III. A comparison with theoretical predictions is given, including frequency dependence. Temperature and electronic density dependences are also investigated. The next section focuses on the dissipative part of the magnetopolarizability of the rings. Theoretical results for this quantity are derived and compared to the experiment. Section V is devoted to the measurements of the magnetic response of the same rings. Despite the fact that the signal is then smaller, the magnetic response of the rings is detected and compared to predictions on averaged persistent currents. We conclude by a comparison between the magnetic and electric response.

II. EXPERIMENTAL SETUP

A. The sample

1. The rings

We have studied the electric and magnetic susceptibilities of isolated Aharonov-Bohm rings. Our system is an array of 10^5 2D rings etched by reactive ion etching in a high-mobility $Al_xGa_{1-x}As/GaAs$ heterojunction. The characteristics of these rings are given in Table I. They are ballistic in the transverse direction and diffusive longitudinally ($l_e<L$ and $l_e\gg W$). It is important to perform a deep etching of the heterojunction (down to GaAs) in order to minimize high-frequency losses, which have been observed to be important in etched $Al_xGa_{1-x}As$. Because of etching the electronic density is strongly depressed. However, we are able to recover the nominal density of the heterojunction by illuminating the rings with a infrared diode placed close to the sample in the dilution refrigerator. For each illumination a current of 10 μA is run through the diode for several minutes. Measurements are done at least 1 h after the illumination in order to ensure good stability of the sample. An upper value of the estimated illumination power coupled to the sample is 600 photons/s with a wavelength of 766 nm. With this setup we are thus able to perform measurements at different electronic densities. The control on the density is rather qualitative because of the difficulty to calibrate the illumination procedure. We have checked the effect of illumination on a connected Aharonov-Bohm (AB) ring (Fig. 1). At zero illumination time the conductance of the ring is zero. On such a sample we can follow the AB oscillations when the resistance decreases by more than an order of magnitude with illumination. As a consequence a clear effect of illuminating the ring is to increase its conductance. The Fourier transform of the resistance of the ring is shown in Fig. 2. We see for each illumination an oscillation whose periodicity is consistent with a flux quantum Φ_0 in the area of the ring. However the Fourier transform shows that the peak corresponding to this periodicity change with illumination both in shape and in amplitude. The amplitude increases with illumination due to the increase of AB oscillations. The fact that the shape, and in particular the width, of the peak change with illumination is an indication that the width of the ring increases with illumination time. To be more precise the width of the rings is multiplied by a factor of 2 between the first and last curve of Fig. 2. Note that the increase of the electronic density has also been shown to induce an increase of the electronic mobility.[20]

In order to study the disorder average we have measured conductance of a single ring and a mesh, representing a two-dimensional square array, etched in the same type of hetero-

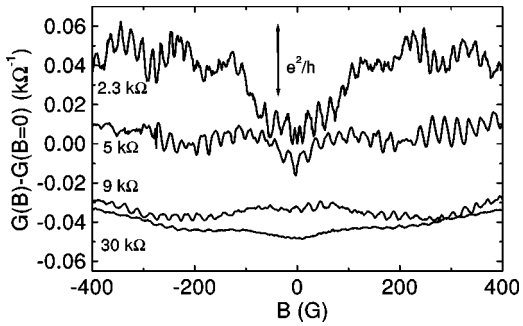

FIG. 1. Conductance of an Aharonov-Bohm ring at different illuminations. At zero illumination the conductance is zero. With illumination the resistance decreases. The curves are shifted for clarity.

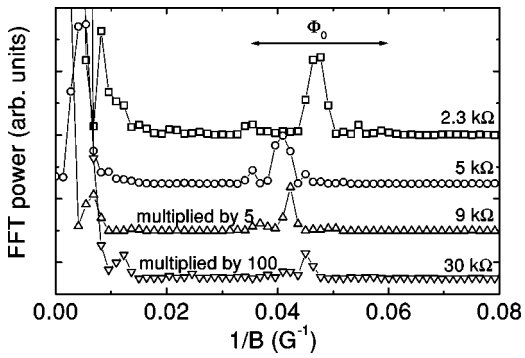

FIG. 2. Fourier transform of the magnetoconductance of an Aharonov Bohm ring at different illumination. The shape and amplitude of the Φ_0 peak are strongly dependent on illumination. The curves are shifted for clarity.

junction than the rings. The magnetoconductance is shown in Fig. 3. As expected the AB effect disappears under ensemble averaging. The $\Phi_0/2$ oscillations, on the other hand, remain on the mesh. In this case the triangular shape of the magnetoconductance is attributed to weak localization in the wire of the mesh.

2. Superconducting microresonator

To measure the electric or magnetic response of the rings we couple them to a superconducting microresonator and detect the changes in its properties. This resonator is made by optical lithography. It consists of a niobium stripline deposited on a sapphire substrate. This substrate has been preferred to silicon or GaAs because it induces the weakest temperature dependence of the resonance frequency and gives the best quality factor due to the quality of the niobium layer on sapphire. A schematic drawing is given in Fig. 4. The width of the wire constituting the resonator is 2 μm, the thickness 1 μm, and the spacing between two adjacent wires 4 μm. The total length of the capacitance or the inductance is 10 or 20 cm. In this kind of resonator the inductance is physically separated from the capacitance by a distance of 300 μm, allowing us to submit the sample only to an electric field (or to a magnetic field) to measure its electric (or magnetic) response. This separation between magnetic and electric response has been checked by deposition of a paramagnetic system (DPPH) alternatively on the capacitive and inductive part of the resonator. A magnetic spin resonance signal was only observed when DPPH was on the inductive part. The resonance frequency of the bare resonator varies between 200 MHz and 400 MHz depending on the geometry. Its quality factor is 10 000 at 4.2 K and 200 000 at 20 mK. The resonator can be modeled by an LC circuit of resistance r, inductance $\mathcal{L}$, and capacitance $\mathcal{C}$, whose resonance frequency is $f_0=(1/2\pi)\sqrt{\mathcal{L}\mathcal{C}}$ and quality factor $Q=\mathcal{L}\omega_0/r$. From the value of the higher resonance frequencies of the resonator we have estimated that the residual capacitance of the meander line is at least 10 times smaller than $\mathcal{C}$. Due to the Meissner effect, the dc field just above the resonator is strongly inhomogeneous. In order to minimize this effect, we have inserted a thin, 1-μm-thick, Mylar film between the detector and the rings. This reduces the field inhomogeneity to about 10%, which is of the order of fluctuations in the lithography.

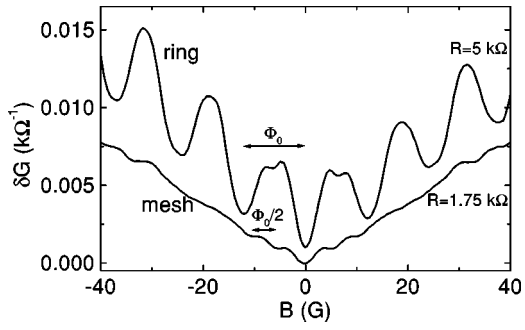

FIG. 3. Magnetoconductance of a ring and a mesh. The Φ_0 signal disappears with ensemble average, so that in the mesh only the $\Phi_0/2$ component remains. Note the triangular shape of the magnetoconductance on the mesh. The curves are shifted for clarity.

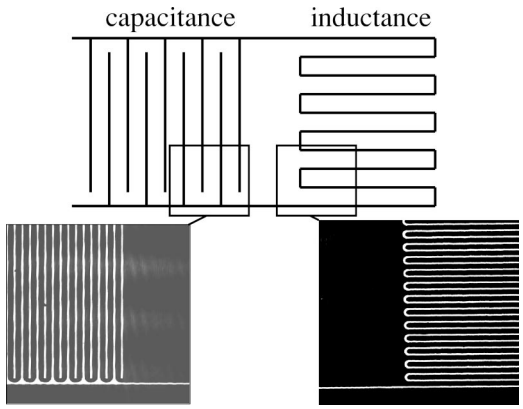

FIG. 4. Schematic drawing of the resonator and optical photographs of part of it. Note that the inductance (meander line) is physically separated from the capacitance (comblike structure).

3. Electric coupling between the rings and the resonator

In order to measure their electric response the rings are placed on top of the capacitance of the resonator. Note that with this procedure the rings are not well aligned with the resonator so that they do not have the same coupling with the capacitance. This is not a problem as only linear response is investigated. We note $\alpha(\omega)=\alpha'(\omega)-i\alpha''(\omega)$ the polarizability averaged over disorder of a ring at the frequency ω. The impedance of the capacitance $\mathcal{C}$ slightly modified by the rings reads

$$Z(\omega)=\frac{1}{i\mathcal{C}\omega[1+Nk_e\alpha(\omega)]}$$

$$\approx\frac{1}{i\mathcal{C}\omega}[1-Nk_e\alpha'(\omega)+iNk_e\alpha''(\omega)].$$

In this expression N is the number of rings coupled to the capacitance and k_e is an averaged coefficient measuring the dielectric coupling between one ring and the capacitance.

The capacitance with the rings is equivalent to a capacitance $\mathcal{C}[1+Nk_e\alpha'(\omega)]$ in series with a resistance $Nk_e\alpha''(\omega)/\mathcal{C}\omega$. Hence

$$\frac{\delta\mathcal{C}}{\mathcal{C}}=Nk_e\alpha'(\omega). \tag{1}$$

The frequency shift due to the rings is then

$$\frac{\delta f}{f_0}=-\frac{1}{2}Nk_e\alpha'(\omega_0). \tag{2}$$

The quality factor is determined by

$$\frac{1}{Q}=\frac{r+\dfrac{Nk_e\alpha''(\omega_0)}{\mathcal{C}\omega_0}}{\mathcal{L}(\omega_0+\delta\omega)}, \tag{3}$$

so that, with $\mathcal{L}\mathcal{C}\omega_0^2=1$ at resonance,

$$\delta\left(\frac{1}{Q}\right)=Nk_e\alpha''(\omega_0)-\frac{1}{Q}\frac{1}{2}k_eN\alpha'(\omega_0)\approx Nk_e\alpha''(\omega_0) \tag{4}$$

provided that $Q\gg 1$.

The electric coupling coefficient is estimated in Appendix B. Knowing this value and the number of rings coupled to the resonator, it is possible to evaluate quantitatively the polarizability of the rings by measuring the resonance frequency shift [Eq. (2)] and the variation of the quality factor [Eq. (4)].

4. Magnetic coupling with the resonator

When the rings are placed on top of the inductance $\mathcal{L}$ of the resonator, this inductance is shifted because of their magnetic response $\chi(\omega)=\chi'(\omega)-i\chi''(\omega)$ according to

$$\frac{\delta\mathcal{L}}{\mathcal{L}}=Nk_m\chi \tag{5}$$

with N the number of rings coupled to the resonator and k_m the magnetic coupling coefficient between one ring and the inductance, which has the dimension of the inverse of a volume. Note that, properly defined, the coupling coefficient k_m is of the same order of magnitude as k_e. More precisely, the estimation of k_e and k_m done in Appendix A leads to $k_m\approx\epsilon_0\epsilon_r k_e$, as expected from Ref. 18. Following the same reasoning as for the electric coupling, the properties of the resonator are modified according to

$$\frac{\delta f}{f}=-\frac{1}{2}Nk_m\chi', \tag{6}$$

$$\delta\left(\frac{1}{Q}\right)=Nk_m\chi''. \tag{7}$$

From previous equations it is in principle possible to measure the absolute value of α or χ. However when a GaAs sample is on the inductive or capacitive part of the resonator, the modification of the resonance is dominated by the influence of the substrate. As a consequence it is very difficult to have an accurate absolute measurement. Nevertheless, relative measurements are possible so that the variation of the electric or magnetic response with magnetic field can be detected in a reliable way.

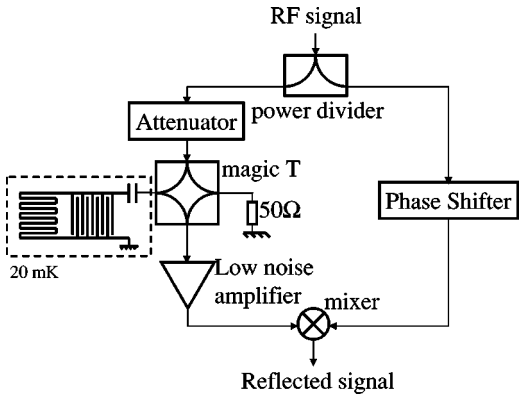

FIG. 5. rf circuit for measuring the reflected signal from the resonator.

B. Measurement of the resonance frequency and the quality factor

The reflected signal of the resonator is measured with the setup of Fig. 5 and used in a feedback loop to lock the frequency of a rf generator to the resonance frequency. The setup is summarized in Fig. 6. The resonator is coupled capacitively to the external circuit using on-chip capacitances. In order to preserve the quality factor of the resonator we work in a configuration where the resonator is undercoupled. The rf power injected is sufficiently low (≈ 10 pW) so as not to heat the sample.

1. Detection of the resonance frequency

The frequency of the rf generator is modulated at Ω and the signal from the resonator is detected by a lock-in detector at the frequency of the modulation. The lock-in signal is to a first approximation the derivative of the resonance peak: it gives an error signal, i.e., this signal is zero at resonance, and changes sign when the frequency of the generator is higher or lower than the resonance frequency. Using this signal in a

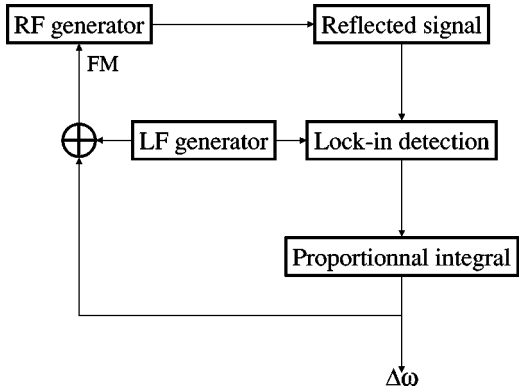

FIG. 6. Experimental setup used to lock the frequency of the rf generator to the resonance frequency.

feedback loop the frequency of the rf generator is locked to the resonance frequency. This way, by measuring the feedback signal, one has direct access to the shift of the resonance frequency. To enhance the accuracy we modulate the magnetic field by a 1-G ac field oscillating at 30 Hz, produced by a small superconducting coil close to the sample, and detect the modulated resonance frequency with a lock-in detector.

2. Detection of the quality factor

At this point we consider that the frequency of the generator is locked to the resonance frequency by the previous setup. The signal measured is the signal reflected from the resonator. As a consequence it is related to the reflexion coefficient $[Z(\omega)-Z_0]/[Z(\omega)+Z_0]$, with $Z(\omega)$ the impedance of the resonator and the coupling capacitance and $Z_0=50\ \Omega$ the impedance matched by the external circuit. We assume that near the resonance frequency the impedance $Z(\omega)$ reads

$$Z(\omega_0+\delta\omega)=\frac{RQ^2}{1+2iQ\,\delta\omega/\omega_0}, \tag{8}$$

with ω_0 the resonance frequency. In the limit $Z(\omega)\ll Z_0$, which corresponds to a very undercoupled resonator, the reflected signal is a linear function of $Z(\omega)$. As a consequence if the rf signal is frequency modulated at Ω around the resonance frequency ω_0 the reflected signal at $2\ \Omega$ is related to the second derivative of the real part $Z(\omega)$, which is proportional to Q^2. In this way, by measuring the signal at $2\ \Omega$ we have access to the quality factor. However, when the frequency modulation is not small compared to the width of the resonance peak or the resonator is not very undercoupled to the external circuit, the relation between the signal at $2\ \Omega$ and the quality factor is not straightforward and needs calibration.

III. FLUX-DEPENDENT POLARIZABILITY

In this part we present measurements of the flux-dependent polarizability of the rings, which are placed on the capacitive part of the resonator as described in Sec. II. In this configuration the resonance frequency is decreased by 15%, due to the dielectric constant of the GaAs substrate. Moreover, the quality factor drops down to 3000 at 20 mK and zero illumination. This strong decrease is attributed to dielectric losses in the heterojunction. The derivative of the resonance frequency of the resonator with the rings is shown on Fig. 7(a). This signal is a straight line, on top of which small oscillations are superimposed. The straight line is due to the field dependence of the penetration length in niobium, which constitutes the resonator. This behavior has been verified to be the same with or without the rings. The oscillating signal is, on the other hand, attributed to the flux-dependent electric response of the rings. These oscillations are extracted by subtracting the base line [Fig. 7(b)]. Note their anharmonicity as well as the existence of an aperiodic signal as illustrated by the Fourier transform of the data [Fig. 7(c)] showing a well-defined peak. In order to focus on this periodic

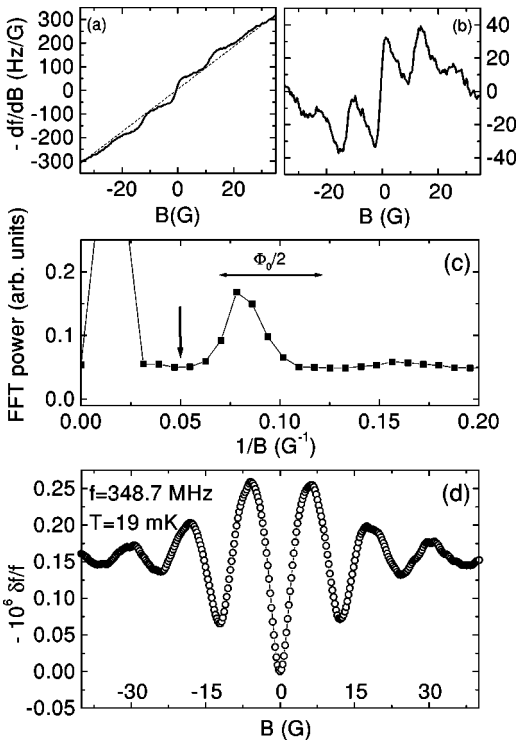

FIG. 7. (a) Derivative of the resonance frequency of the resonator with the rings versus magnetic field at illumination time 870 s. (b) Signal obtained by subtracting the base line [dashed-line on graph (a)] due to the resonator from previous data. (c) Fourier transform of signal (b). The vertical arrow indicates the cutoff frequency used for high-pass filtering the signal. (d) Frequency shift due to the rings obtained after integration of the high-pass filtered signal of (b).

contribution, which is the expected signature of phase coherence, a numerical high-pass filter with a cutoff frequency of $0.05\ \mathrm{G}^{-1}$ [corresponding to the arrow on Fig. 7(c)] is applied and the signal is then numerically integrated in order to have the frequency shift due to the rings [Fig. 7(d)]. This shift is proportional to the variation of polarizability versus magnetic field according to formula (2). We will return to the aperiodic signal in the section devoted to illumination effect.

A. Magnetopolarizability

The frequency shift due to the rings is periodic with a period of approximately 12.5 G. From the Fourier transform [Fig. 7(c)] the period of the oscillation is deduced to be consistent with half a flux quantum $\Phi_0/2$ in a ring with no signature of Φ_0 periodicity, as expected for an Aharonov-Bohm effect averaged over many rings.[23] Note the extra broadening (by more than a factor 2) of this $\Phi_0/2$ peak compared to the measurements on a single connected ring. We interpret this as resulting from the dispersion in circumfrences in the different rings. The sign of frequency shift is negative at low magnetic field, which means according to formula (2) that the magnetopolarizability is positive, i.e., $\alpha'(H)-\alpha'(0)>0$ at low magnetic field. The screening is thus better when time-reversal symmetry is broken by magnetic field. The scale of the signal is given by the amplitude

of the first oscillation. From Fig. 7(d) we deduced $\delta_\Phi f/f = [f(6.3G) - f(0)]/f = -2.5\times10^{-7}$. Note that this value means detecting a frequency shift of 100 Hz at a frequency of 350 MHz. With the coupling coefficient estimated in Appendix B it leads to the value of the magnetopolarizability $\delta_\Phi \alpha'/\alpha_{1D} = 5\times10^{-4} \pm 2.3\times10^{-4}$, where $\alpha_{1D} = \epsilon_0 \pi^2 R^3/\ln(R/W)$ is the calculated polarizability of a quasi-one-dimensional (quasi-1D) circular ring of radius R.

B. Theoretical predictions

Our experiment shows that there is a flux correction to the polarizability of the rings, which is *positive* at low field. Let us now compare this result to recent theoretical predictions. Since we are using a ring geometry we are going alternatively from a situation where the system presents time-reversal symmetry (at flux values of $\Phi = n\Phi_0/2$, with $n \in \mathbb{Z}$) to the case where time reversal symmetry is broken by magnetic field. In the random matrix theory (RMT) the first case corresponds to the Gaussian orthogonal ensemble (GOE) whereas the second is related to the Gaussian unitary ensemble (GUE). So the quantity to be compared with theoretical predictions that evaluate the variation of a physical variable A between GOE and GUE is $\delta_\Phi A$, defined as $A(\Phi_0/4) - A(0)$. Note that since the rings are semiballistic, the transition with magnetic field may not be exactly from GOE to GUE.

The polarizability of small metallic grains was studied using RMT first by Gor'kov and Eliashberg.[24] The sensitivity of the electrostatic properties of mesoscopic systems to quantum coherence has been emphasized by Büttiker for connected geometries.[25] The phase-coherent correction to the polarizability of isolated systems was recently theoretically investigated. Efetov found that it is possible to relate this correction self-consistently to the flux dependence of the screened potential.[15] Two recent works have calculated this effect in the diffusive regime using linear response formalism (Noat *et al.*[16,26]) or supersymmetry techniques (Blanter and Mirlin[17,27]).

In the grand canonical ensemble (GCE) the chemical potential in each ring is supposed to be constant. It describes a situation where the rings are connected to a reservoir of particules. *A priori* this is not the case in the experiment where the rings are isolated, but as the theory is simpler in GCE we recall first the result in this statistical ensemble. No flux dependence for the polarizability is predicted if the rf pulsation ω is much smaller than the inverse relaxation time γ. However, when $\omega \gg \gamma$ the magnetopolarizability is related to the flux dependence of the diagonal matrix element of the screened potential:

$$\delta_\Phi \alpha'_{\mathrm{GCE}} = -\frac{2e^2}{E^2\Delta}\,\delta_\Phi(\langle |F_{\alpha\alpha}|^2\rangle_\mu). \tag{9}$$

$\langle |F_{\alpha\alpha}|^2\rangle_\mu$ is the disorder averaged squared of the diagonal matrix element of the screened potential F at energy μ, the mean chemical potential of the rings. E is the applied electric field. ψ_α are the eigenstates of the unperturbed system. This matrix element is then given by

$$\langle |F_{\alpha\alpha}|^2\rangle_\mu = \int d\mathbf{r}_1 \int d\mathbf{r}_2 F(\mathbf{r}_1)F(\mathbf{r}_2)\langle |\psi_\alpha(\mathbf{r}_1)\psi_\alpha(\mathbf{r}_2)|^2\rangle_\mu . \tag{10}$$

From this expression it appears that the magnetopolarizability is related to the difference of the correlation function of the eigenstates with and without time-reversal symmetry. This correlation function has been computed in the diffusive regime within a supersymmetric σ-model approach:[28,29]

$$V^2\langle |\psi_\alpha(\mathbf{r}_1)\psi_\alpha(\mathbf{r}_2)|^2\rangle_\mu = [1 + 2k_d(r)] \times [1 + 2\Pi_D(\mathbf{r}_1,\mathbf{r}_2)] \quad \text{(GOE)}, \tag{11}$$

$$V^2\langle |\psi_\alpha(\mathbf{r}_1)\psi_\alpha(\mathbf{r}_2)|^2\rangle_\mu = [1 + k_d(r)] \times [1 + \Pi_D(\mathbf{r}_1,\mathbf{r}_2)], \quad \text{(GUE)} \tag{12}$$

with V the volume of the sample, $k_d(r)$ a short-range function that decays on the length scale of the mean free path, and $\Pi_D(\mathbf{r}_1,\mathbf{r}_2)$ the diffusion propagator. The correction due to the short-range term $k_d(r)$ has been shown to be negligible.[17] By considering only the diffusion term the magnetopolarizability is given by

$$\delta_\Phi \alpha'_{\mathrm{GCE}} = \frac{2e^2}{E^2\Delta V^2}\int d\mathbf{r}_1 \int d\mathbf{r}_2 F(\mathbf{r}_1)F(\mathbf{r}_2)\Pi_D(\mathbf{r}_1,\mathbf{r}_2). \tag{13}$$

Note that this derivation of the magnetopolarizability is equivalent to the one used by Noat *et al.*[16] based on the following RMT argument:

$$\delta_\Phi(\langle |F_{\alpha\alpha}|^2\rangle) \approx -\frac{1}{2}\langle |F_{\alpha\alpha}|^2\rangle_{\mathrm{GOE}}. \tag{14}$$

This relation can also be obtained from Eqs. (11) and (12) using the fact that

$$\int d\mathbf{r}\, F(\mathbf{r}) = 0 \tag{15}$$

due to symmetry properties of the screened potential. The calculation of the magnetopolarizability using formula (13) for the case of a quasi-1D ring (Appendix C) leads to

$$\frac{\delta_\Phi \alpha'_{\mathrm{GCE}}}{\alpha_{1D}} = \epsilon_r f\left(\frac{L}{W}\right)\frac{\lambda_s}{W}\frac{\Delta}{E_c}. \tag{16}$$

$f(x)$ is a function related to the geometry and the dimension of the sample. Using this expression and the value of Table I we have $\delta\alpha'_{\mathrm{GCE}}/\alpha_{1D} = 1.2\times10^{-3}$.

In our experiment the rings are isolated and the number of electrons in each ring is supposed to be constant, so that the result of the canonical ensemble (CE) should apply. At $T = 0$ and zero frequency the flux-dependent correction to polarizability is found to be zero. However, at $\omega \gg \Delta$ the GCE result is recovered. The complete frequency dependence of the magnetopolarizability in the CE has been recently derived by Blanter and Mirlin.[27] Following their reasoning but taking into account the level broadening γ we can write

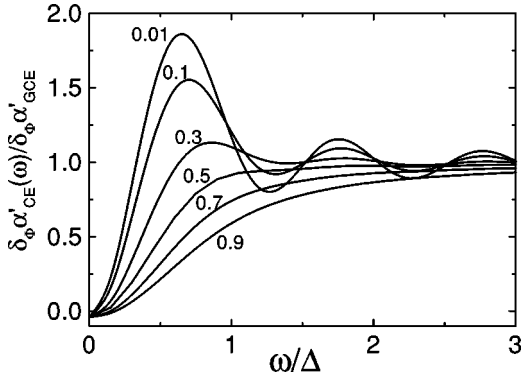

FIG. 8. Calculated evaluation of $\delta_\Phi\alpha'_{\mathrm{CE}}(\omega)/\delta_\Phi\alpha'_{\mathrm{GCE}}$ at different value of the parameter γ/Δ. Note that the value of magnetopolarizability is zero at zero whatever the level broadening.

$$\delta_\Phi\alpha'_{\mathrm{CE}}(\omega)=\delta_\Phi\alpha'_{\mathrm{GCE}}F(\omega) \tag{17}$$

with $F(\omega)$ a function that depends only on the statistic of energy levels:

$$F(\omega)=1+\int_0^\infty d\epsilon\frac{1}{\epsilon}\left(\frac{\epsilon(\epsilon+\omega)+\gamma^2}{(\epsilon+\omega)^2+\gamma^2}+\frac{\epsilon(\epsilon-\omega)+\gamma^2}{(\epsilon-\omega)^2+\gamma^2}\right)$$
$$\times\left[\delta_\Phi R_2(\epsilon)+\int_0^\epsilon d\epsilon_1\delta_\Phi R_3(\epsilon,\epsilon_1)\right]. \tag{18}$$

$R_2(\epsilon)$ and $R_3(\epsilon,\epsilon_1)$ are, respectively, the two- and three-level correlation function, known from RMT.[30,31] By evaluating this expression versus frequency at different values of level broadening we get the results shown in Fig. 8.

The behavior at low values of the level broadening is in qualitative agreement with result of Ref. 27. In particular the magnetopolarizability is found to be zero at zero frequency [in our calculation the value of $\delta_\Phi\alpha'_{\mathrm{CE}}(\omega=0)$ is at least 25 times smaller than $\delta_\Phi\alpha'_{\mathrm{GCE}}$]. The present experiment was performed at $\omega/\Delta=0.2$, and the CE magnetopolarizability is equal at most to 50% of the GCE value (in the limit of small level broadening). As a consequence the expected value for $\delta_\Phi\alpha'_{\mathrm{CE}}/\alpha_{1\mathrm{D}}$ is then 6×10^{-4}, which is of the same order of magnitude as the experimental value. Note that the measurement is not sufficiently accurate to give an estimate of the level broadening by comparing the experimental result with the curves of Fig. 8. A very interesting extension of the experiment would be to study the magnetopolarizability at different frequencies in order to test the theoretical predictions. This could be done by working with resonators with smaller inductances.

C. Effect of temperature

The temperature dependence of the signal is also investigated. The magnetopolarizability decreases with temperature (inset of Fig. 9). Theoretically the effect of temperature on magnetopolarizability has not been studied yet. We will base our analysis of the temperature dependence on the hypothesis that the amplitude of the signal is related to the phase-coherence length L_Φ in the same way as weak localization. In this case the amplitude of the $\Phi_0/2$ component of the signal is proportional to $\exp[-2L/L_\Phi(T)]$.[4] In Fig. 9 the temperature dependence of this component is shown. We have tried to fit it using two laws for $L_\Phi(T)$. First, using the behavior deduced from the measurements on connected wires[32] we have tried the experimental value $L_\Phi^{\mathrm{expt}}(T)$, which exhibits a $T^{-1/3}$ dependence, as expected for 1D systems.[33] It leads to poor agreement with experimental points. Using for the phase-coherence time the result of electron-electron interaction in quantum dots (0D system[34]) $\tau_\Phi(T)\propto T^{-2}$, leading in the diffusive regime to $L_\Phi(T)\propto 1/T$, gives better agreement. In this case the temperature scale is found to be 90 mK. We deduced from this value $\gamma=1/\tau_\Phi=D/L_\Phi^2\simeq 0.8$ mK at 18 mK, i.e., much smaller than the level spacing. The phase-coherence length deduced from this analysis is 10 times higher than the length measured on the connected sample.[32] We relate this difference between the nonconnected and connected case to the fact that whereas the connected samples are one dimensional with a continuous energy spectrum due to the strong coupling with the reservoirs, the spectrum of the nonconnected rings is discrete. As a concluding remark on this temperature dependence, we want to emphasize the need for a deeper theoretical analysis on the behavior of the magnetopolarizability versus temperature.

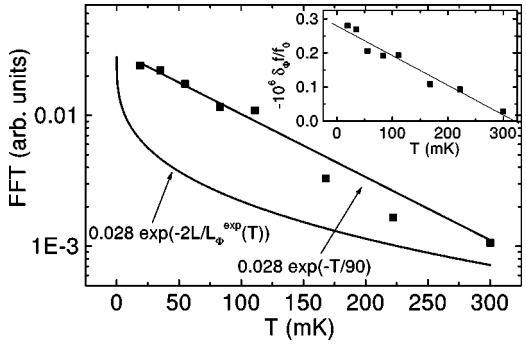

FIG. 9. Temperature dependence $\Phi_0/2$ component of the Fourier transform of the signal. The fitting function used is proportional to $\exp[-2L/L_\Phi(T)]$ with two fitting functions for $L_\Phi(T)$. First we took the phase-coherence length measured on connected sample $L_\Phi^{\mathrm{expt}}(T)$, which exhibits a $T^{-1/3}$ behavior. The other fitting function is $L_{\Phi(T)}\propto 1/T$. The best agreement is found with an exponential decay with a temperature scale of 90 mK. Inset: Temperature dependence of the frequency shift due to the rings.

D. Effect of illumination

Using the procedure described in Sec. II A 1 we are able to study the influence of electronic density on magnetopolarizability. In Fig. 10 the Fourier transform of the derivative of frequency shift, when the baseline due to the resonator is removed, is shown at different illumination times. As expected the Fourier transform exhibits a $\Phi_0/2$ peak. Note also the low-frequency component that corresponds to the aperiodic signal seen in Fig. 7(b). The $\Phi_0/2$ peak depends on electronic density. Its amplitude shows first an increase and then decreases at high illumination. Moreover the width of the $\Phi_0/2$ peak increases, showing that the rings widen with illumination. The peak becomes asymmetric, suggesting that

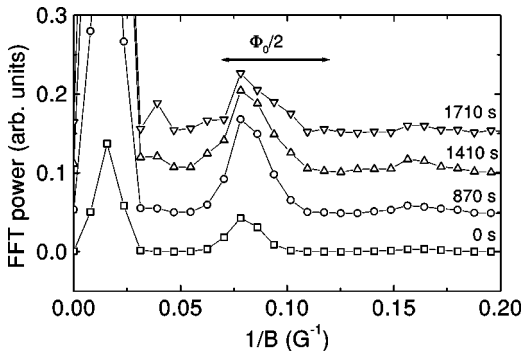

FIG. 10. Fourier transform of the derivative of the resonance frequency versus magnetic field at different illumination. The curves are shifted for clarity.

rings having long circumferences initially not populated contribute to the signal at high illumination. Following the procedure described in Sec. III we measured the amplitude of magnetopolarizability versus illumination time. It yields Fig. 11, which shows the change of the amplitude of the magnetopolarizability. At first the signal increases, then for illumination time above 1400 s the amplitude of oscillation decreases. We interpret this behavior in the following way. Before illumination the electronic density in the rings obtained after deep etching of the 2D electron gas (2DEG) is strongly depressed compared to the nominal value. As a consequence an important fraction of the rings is likely to be localized and does not contribute to the magnetopolarizability. In this regime the signal is small. After illumination the number of rings contributing to the signal increases so that the frequency shift due to the rings increases. At high enough electronic density when the rings are sufficiently populated so that they contain delocalized electrons the theoretical results obtained in the diffusive regime are expected to be valid, leading to a $1/g$ dependence [formula (16)], with $g = E_c/\Delta$ the dimensionless conductance. This is a possible explanation for the decrease of the magnetopolarizability observed at high illumination level. Note that we cannot exclude also a reduction of the screening length λ_s due to illumination. From formula (16) we deduce then a decrease of the signal. However, we believe that the screening length changes very weakly with illumination because this length is

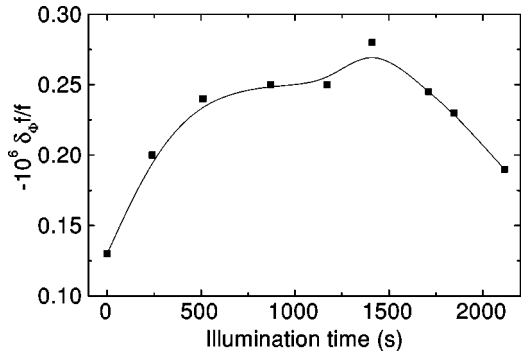

FIG. 11. Amplitude of the frequency shift due to the rings at different illumination time.

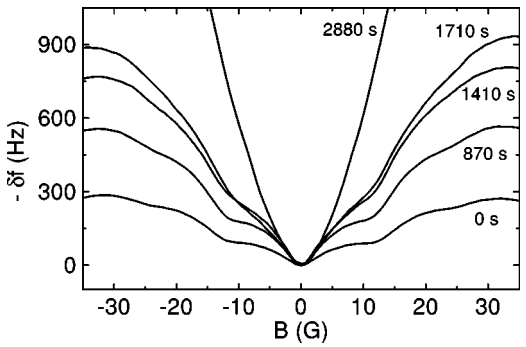

FIG. 12. Frequency shift without selecting the $\Phi_0/2$ component before numerical integration, for different illumination times.

essentially determined by the density of states at the Fermi energy, which is independent of energy for a 2D system (see Table I).

We have analyzed so far the $\Phi_0/2$ periodic component of the magnetopolarizability signal obtained after filtering low frequency (see Fig. 7). On the other hand, the whole integrated signal is depicted in Fig. 12. One can clearly see a triangular shape dependence of the signal with magnetic field superimposed on the oscillations, very similar to the weak-localization conductance of the connected mesh shown in Fig. 3. Note that this behavior is only present at low temperature; it completely disappears for temperatures higher than 300 mK. The amplitude of this extra signal due to the finite width of the rings strongly increases and sharpens with illumination. We think that it is reasonable to attribute this evolution to the increase of the width of the rings. Note that a similar evolution has been previously observed in the ac magnetoconductance of ballistic GaAs squares.[35]

IV. ELECTRIC ABSORPTION

By measuring the quality factor of the resonator versus magnetic field, we have access to the flux-dependent electric absorption [formula (4)], which is related to the conductance, in the case of an electric dipole, through

$$G_e = \frac{\omega \alpha''}{a^2}. \tag{19}$$

The contribution due to the rings (Fig. 13) exhibits the same

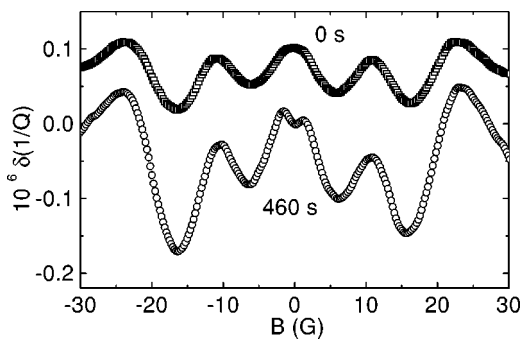

FIG. 13. Variation of $1/Q$ versus magnetic field at different illumination.

periodicity as the frequency shift, which corresponds to half a quantum flux in a ring. The low-field signal decreases. It corresponds to a negative magnetoconductance, i.e., opposite to weak localization. This surprising sign was pointed out in the context of the magnetoconductance of rings submitted to an oscillating magnetic flux in the discrete spectrum limit.[36–38]

To explain this result one has to take into account the level spacing distribution in a disordered system.[24,39] The sign and amplitude of the typical variation of electric absorption are understandable using the fact that level repulsion in a disordered system is higher in GUE than in GOE. Following Ref. 18 the flux-dependent electric absorption in a system described by eigenvalues ϵ_α and the corresponding eigenfunctions ψ_α could be written in a linear response regime,

$$\delta_\Phi \alpha'' = -\frac{2e^2}{E^2}\delta_\Phi\left(\sum_{\alpha\neq\beta}\frac{f_\alpha - f_\beta}{\epsilon_{\alpha\beta}}\frac{\gamma\omega}{(\epsilon_{\alpha\beta}+\omega)^2+\gamma^2}|F_{\alpha\beta}|^2 + \frac{\gamma\omega}{\gamma^2+\omega^2}\sum_\alpha\frac{\partial f_\alpha}{\partial\epsilon_\alpha}|F_{\alpha\alpha}|^2\right), \tag{20}$$

with $\epsilon_{\alpha\beta}=\epsilon_\alpha-\epsilon_\beta$. We will first consider this expression in the GCE where an average over the chemical potential is computed. With this procedure $\langle(f_\alpha-f_\beta)/(\epsilon_{\alpha\beta})\rangle=-1/\Delta\mu$ and $\langle\partial f_\alpha/\partial\epsilon_\alpha\rangle=-1/\Delta\mu$, where $\Delta\mu$ is the range over which the average over the chemical potential is done. The first term in the right-hand side of Eq. (20) then reads

$$\frac{2e^2}{E^2\Delta\mu}\delta_\Phi\left(\sum_{\epsilon_\alpha\neq\epsilon_\beta}\frac{\gamma\omega}{(\epsilon_{\alpha\beta}+\omega)^2+\gamma^2}|F_{\alpha\beta}|^2\right). \tag{21}$$

Note that in this sum the energies ϵ_α and ϵ_β have to belong to the range $[\mu-\Delta\mu/2,\mu+\Delta\mu/2]$. Using this constraint we replace the sum by an integral,

$$\sum_{\epsilon_\alpha<\epsilon_\beta}(\,) = \frac{\Delta\mu}{\Delta}\int_0^\infty\frac{d\epsilon}{\Delta}R_2(\epsilon)(\,), \tag{22}$$

with $R_2(\epsilon)$ the two-energy-level correlation function. In this expression we neglect the flux dependence of the matrix element and note its average value $\langle|F_{\alpha\beta}|^2\rangle_{\mu,\omega}$. With this approximation Eq. (21) reads

$$\frac{2e^2}{E^2\Delta}\langle|F_{\alpha\beta}|^2\rangle_{\mu,\omega}\int_0^\infty\frac{d\epsilon}{\Delta}\left(\frac{\gamma\omega}{(\epsilon+\omega)^2+\gamma^2}+\frac{\gamma\omega}{(\epsilon-\omega)^2+\gamma^2}\right)\delta_\Phi R_2(\epsilon). \tag{23}$$

The Debye term of Eq. (20) is equal in the GCE to

$$\frac{2e^2}{E^2\Delta}\frac{\gamma\omega}{\omega^2+\gamma^2}\delta_\Phi(|F_{\alpha\alpha}|^2). \tag{24}$$

In the GCE in the dynamical regime the flux correction to the polarizability is given by formula (9) at $T=0$. Using the following correlation function,[29]

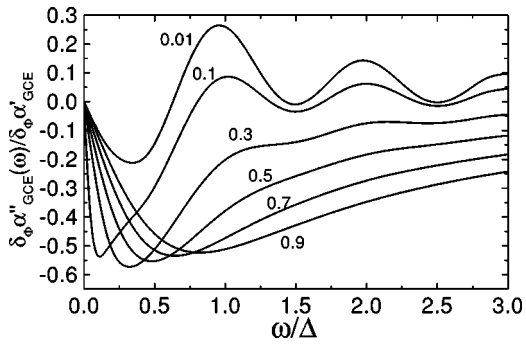

FIG. 14. Calculated value of $\delta_\Phi\alpha''_{\rm GCE}(\omega)/\delta_\Phi\alpha'_{\rm GCE}$ versus ω in GCE at different value of the parameter γ/Δ.

$$V^2\langle\psi^*_\alpha(\mathbf{r}_1)\psi_\beta(\mathbf{r}_1)\psi_\alpha(\mathbf{r}_2)\psi^*_\beta(\mathbf{r}_2)\rangle_{\mu,\omega} = k_d(\mathbf{r})+[1+k_d(\mathbf{r})]\Pi_D(\mathbf{r}_1,\mathbf{r}_2) \quad \text{(GOE)}, \tag{25}$$

we have $\delta_\Phi(\langle|F_{\alpha\alpha}|^2\rangle_\mu)\approx-\langle|F_{\alpha\beta}|^2\rangle^{\rm GOE}_{\mu,\omega}$. Hence

$$\frac{\delta_\Phi\alpha''_{\rm GCE}(\omega)}{\delta_\Phi\alpha'_{\rm GCE}} = -\frac{\gamma\omega}{\omega^2+\gamma^2}+\int_0^\infty\frac{d\epsilon}{\Delta}\left(\frac{\gamma\omega}{(\epsilon+\omega)^2+\gamma^2}+\frac{\gamma\omega}{(\epsilon-\omega)^2+\gamma^2}\right)\delta_\Phi R_2(\epsilon), \tag{26}$$

which can be evaluated numerically (Fig. 14).

For isolated rings we have to apply the result of CE. It is then possible to estimate the correction to electric absorption by using the same treatment as for the real part of polarizability. It leads to

$$\frac{\delta_\Phi\alpha''_{\rm CE}(\omega)}{\delta_\Phi\alpha'_{\rm GCE}} = \int_0^\infty\frac{d\epsilon}{\Delta}\frac{1}{\epsilon}\left(\frac{\omega\gamma}{(\epsilon+\omega)^2+\gamma^2}+\frac{\omega\gamma}{(\epsilon-\omega)^2+\gamma^2}\right)\times\left[\delta_\Phi R_2(\epsilon)+\int_0^\epsilon d\epsilon_1\delta_\Phi R_3(\epsilon,\epsilon_1)\right]. \tag{27}$$

Numerical estimation of this formula at different values of the level broadening leads to the behavior shown in Fig. 15. The electric absorption is always negative at low frequency and may change sign at low values of γ/Δ.

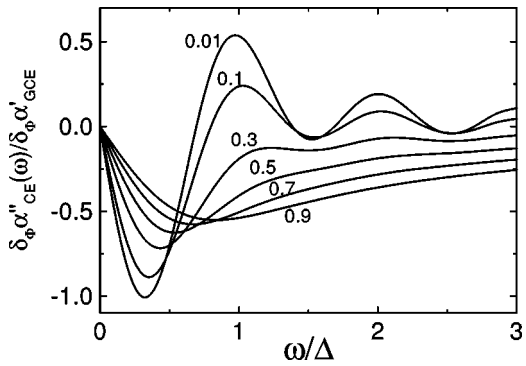

FIG. 15. Calculated electric absorption in CE versus frequency at different value of the parameter γ/Δ.

In order to compare these calculations with our experimental result we will compute the ratio $\delta_\Phi\alpha''/\delta_\Phi\alpha'$. It is worth noting that in our experiment this quantity is given according to Eqs. (2) and (4) by $\delta_\Phi(1/Q)/(-2\delta_\Phi f/f)$ and is independent of the number of rings coupled to the resonator or the electric coupling coefficient k_e. Experimentally we find $\delta_\Phi\alpha''/\delta_\Phi\alpha' = -0.2$ at illumination time zero and -0.23 after 420 s of illumination. Theoretically, at $\omega/\Delta = 0.2$, $\delta_\Phi\alpha'_{\mathrm{CE}}(\omega) = 0.5\delta_\Phi\alpha'_{\mathrm{GCE}}$ and $\delta_\Phi\alpha''(\omega)/\delta_\Phi\alpha'_{\mathrm{GCE}} = -0.5$ so that the expected value of $\delta_\Phi\alpha''(\omega)/\delta_\Phi\alpha'_{CE}(\omega)$ is around 1. It corresponds to small γ/Δ. For higher values of this parameter the ratio is of the same amplitude or higher. As a consequence the predicted behavior is consistent with the experimental value for the sign, but the theoretical amplitude is too high by more than a factor of 2. This conclusion is different from our previous statement where the frequency dependence of the real part of magnetopolarizability was not taken into account.[19]

V. MAGNETIC RESPONSE

Due to the design of the resonator we have also the opportunity to investigate the magnetic response of the same Aharonov-Bohm rings used for the measurements of the electric response. In this case the rings are placed on top of the inductive part of the resonator. Note that to do so we have to warm up, cool down, and reilluminate the rings. As a consequence, strictly speaking, the rings are not the same as for the measurement of the electrical response because the electronic density and the disorder realization in each ring are not exactly the same from one run to the other. Nevertheless, due to the fact that we are measuring an ensemble average quantity, the change in disorder realization of each ring does not modify the result of the experiment. Moreover, we have checked (on the electric response measurement) that, for the same illumination procedure, the result varies within a 15% range from one run to the other. The flux-dependent orbital magnetism at a frequency of 350 MHz is then detected. In this configuration the quality factor of the resonator is only 500. We do not understand this strong increase of magnetic losses. This low-quality factor decreases the accuracy of our measurements of the resonance frequency. Moreover, it prevents precise measurements of the flux dependence of the dissipative part of magnetic response of the rings. As a consequence in this part we present only the flux-dependent nondissipative part of the magnetic response. Note that we cannot rule out the fact that the signal measured in this configuration could be partially due to electric response of the rings. However, due to the small value of the residual capacitance of the meander line and the bad electric coupling in this geometry this electric component is estimated to be at least 20 times smaller than when the rings are placed on top of the capacitance. Moreover, the very different shape of the electric and magnetic signals is strong evidence that we are indeed measuring essentially the magnetic response of the rings.

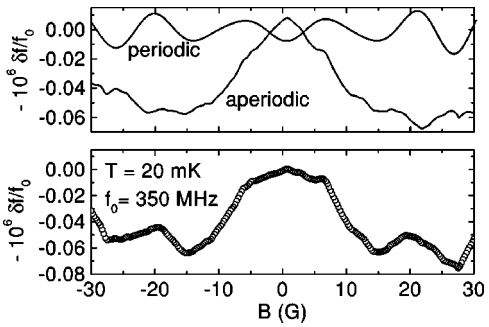

FIG. 16. Lower part: frequency shift due to the rings at 20 mK and zero illumination time. Upper part: the previous signal is decomposed into a periodic behavior and a low-frequency behavior.

A. Flux-dependent orbital magnetism

The signal measured at zero illumination, after subtracting the baseline due to the resonator, is shown in the lower part of Fig. 16. Inspired by our previous analysis we decompose the measured field-dependent part of the signal into an aperiodic and a periodic part, which corresponds to $\Phi_0/2$ in a ring (Fig. 16). We interpret the $\Phi_0/2$ component as the contribution of electronic trajectories enclosing the whole ring. On the other hand, the triangular shape signal could be due to the contribution of trajectories confined in the finite width of the ring. The amplitude of the $\Phi_0/2$ periodic component of the signal is $\delta_\Phi f/f = -1.5\times10^{-8}$. We deduce from formula (6) and evaluation of the magnetic coupling done in Appendix A that the flux-dependent magnetic response of the ring is $\delta_\Phi\chi = 5.4\times10^{-24} \pm 2.1\times10^{-24}\mathrm{m}^{-3}$. In the following we first assume that the main contribution to this signal is due to the flux derivative of the persistent currents[40] and then discuss finite frequency effects. If the flux dependence of persistent currents is $I(\Phi) = I_0 \sin(4\pi\Phi/\Phi_0)$, we deduce

$$I_0 = -\frac{\delta_\Phi\chi}{2\mu_0}\frac{\Phi_0}{4\pi S^2}, \tag{28}$$

with S the surface of the ring. We find then a *diamagnetic* average persistent current, the amplitude of which is $|I_0| = 0.25 \pm 0.1$ nA. The aperiodic component of the signal corresponds, on the other hand, to low-field paramagnetism.

B. Persistent currents

Let us now compare our result for the average persistent currents to other experimental results and to theoretical predictions. A $\Phi_0/2$ periodic diamagnetic persistent current has been also observed in arrays of metallic rings.[11,13] The expected amplitude of the averaged current due to repulsive electron-electron interactions from the first-order Hartree-Fock calculation[41] is $E_c/\Phi_0 = 1.5$ nA, this value is expected to be decreased by higher-order terms. Considering, on the other hand, theoretical predictions for noninteracting electrons[42] the expected value is between $\sqrt{\Delta E_c}/\Phi_0 = 0.6$ nA and $\Delta/\Phi_0 = 0.3$ nA. In both cases the currents are predicted to be paramagnetic. The rather small difference between interacting and noninteracting electrons is very specific to the GaAs rings where the number of electrons is small. The mea-

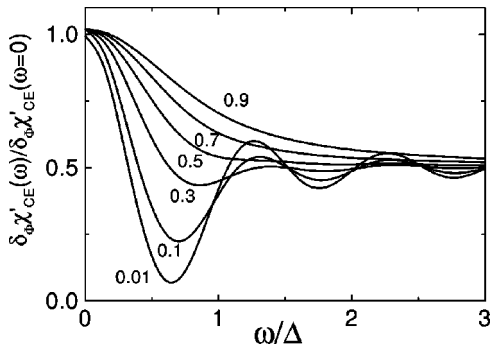

FIG. 17. Calculated frequency dependence of the real part of the susceptibility at different values of the parameter γ/Δ.

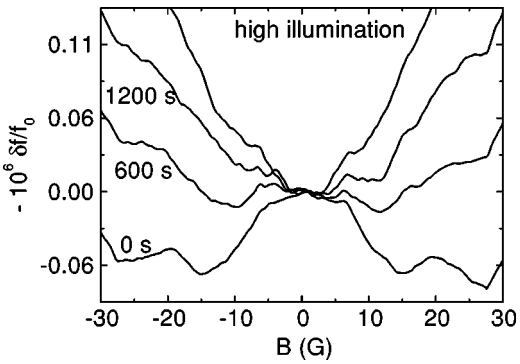

FIG. 18. Frequency shift due to the magnetic response of the rings at different illumination time.

sured signal is consistent for the amplitude but not for the sign (unless assuming attractive interactions) with theoretical predictions.

It may also be important to take into account an effect of frequency for the flux-dependent orbital magnetism. In fact by applying a formalism very similar to the one used for magnetopolarizability the variation of the real part (nondissipative) of the susceptibility of a ring submitted to an oscillating magnetic flux in CE without interactions is given by[36,40]

$$\delta_\Phi\chi'(\omega)=\delta_\Phi\left(\sum_{\alpha\neq\beta}\frac{f_\alpha-f_\beta}{\epsilon_{\alpha\beta}}\frac{\epsilon_{\alpha\beta}(\epsilon_{\alpha\beta}+\omega)+\gamma^2}{(\epsilon_{\alpha\beta}+\omega)^2+\gamma^2}|J_{\alpha\beta}|^2\right) \tag{29}$$

with $J_{\alpha\beta}$ the matrix element of the current operator. It is then possible to apply the same reasoning as for the real part of polarizability, and to use the fact that $\delta_\Phi(\langle|J_{\alpha\alpha}|^2\rangle)=\langle|J_{\alpha\beta}|^2\rangle$, so that

$$\frac{\delta_\Phi\chi'(\omega)}{\delta_\Phi\chi'(\omega=0)}=\frac{1}{2}\left\{1-\int_0^\infty d\epsilon\frac{1}{\epsilon}\left(\frac{\epsilon(\epsilon+\omega)+\gamma^2}{(\epsilon+\omega)^2+\gamma^2}+\frac{\epsilon(\epsilon-\omega)+\gamma^2}{(\epsilon-\omega)^2+\gamma^2}\right)\left[\delta_\Phi R_2(\epsilon)+\int_0^\epsilon d\epsilon_1\delta_\Phi R_3(\epsilon,\epsilon_1)\right]\right\}. \tag{30}$$

The evaluation of this expression is easily deduced from the evaluation of magnetopolarizability and leads to Fig. 17. Frequency induces a strong decrease of the magnetic signal for frequencies of the order of Δ but does not seem to induce a sign change of $\delta_\Phi\chi'$. Note that in strong contrast with the electric response the magnetic susceptibility is maximum at zero frequency, which corresponds to persistent currents. It would be important to investigate the effect of finite frequency on the contribution due to electron-electron interactions on persistent currents.

Recently it has been suggested that the measured currents may be due to a rectifying behavior of the rings: a high-frequency noise leads then to a dc current.[43] Noise also induces dephasing. A recent paper by Kravtsov and Altshuler[44] predicts that those two quantities, average persistent current and dephasing measured by the saturation of the phase coherence time, are related in a simple way: $I=Ce/\tau_\Phi(T=0)$. C is a constant giving the sign of the persistent current and $\tau_\Phi(T=0)$ the dephasing time at zero temperature. Using the value of $\tau_\Phi=1.5$ ns at 20 mK, deduced from measurements on the connected sample, and considering the orthogonal case (absences of spin orbit, then $C=-4/\pi$), we deduce an expected value for persistent currents of -0.14 nA. The predicted persistent current is then *diamagnetic*. The sign and amplitude are then consistent with our experimental findings. On the other hand, if we take the value deduced from the temperature dependence of the magnetopolarizability of nonconnected rings, which is not the case considered theoretically, we deduce $I_0=-0.02$ nA, smaller by an order of magnitude than the experimental value.

C. Effect of illumination

The influence of electronic density on the magnetic response of the rings has been investigated by illuminating them. Different illumination times are shown in Fig. 18. We observed that the triangular envelope of the signal changes sign and increases with illumination. For each illumination the Fourier transform of the signal exhibits a component that is consistent with half a flux quantum periodicity (Fig. 19). One sees, however, that with illumination the shape of the $\Phi_0/2$ peak in the Fourier transform is modified. The peak broadens with electronic density, indicating that the width of the rings increases. Note that this width is always consistent

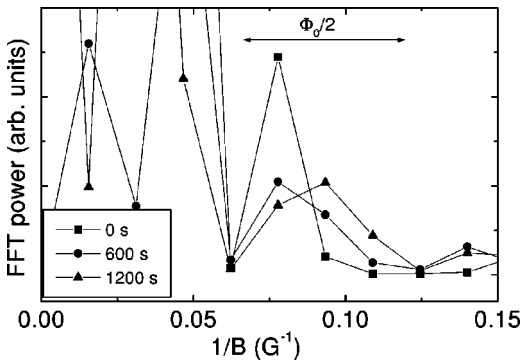

FIG. 19. Fast Fourier transform of the magnetic response of the rings at different illumination.

with the one deduced from etching and depletion effects. The power of the Fourier transform integrated in the $\Phi_0/2$ zone is constant within 10%. So the amplitude of the $\Phi_0/2$ signal is constant but its shape is modified. It indicates that the amplitude of the persistent currents does not depend much on electronic density. The sign change of the low-frequency part of the flux-dependent magnetic response of the rings, going from low-field paramagnetism to diamagnetism, is not understood.

VI. CONCLUSION

We have presented measurements of electric and magnetic responses of Aharonov-Bohm rings etched in a 2DEG. They present a flux-dependent correction to screening. This correction is positive in low field which means that screening is enhanced when time-reversal symmetry is broken by a magnetic field. The sign of the effect is consistent with theory for isolated rings at finite frequency. The value of magnetopolarizability is $\delta_\Phi \alpha'/\alpha_{1D}=5\times10^{-4}\pm2.3\times10^{-4}$, with $\alpha_{1D}=\epsilon_0\pi^2R^3/\ln(R/W)$ the calculated polarizability of a quasi-1D circular ring of radius R. The temperature dependence of magnetopolarizability is consistent with $L_\Phi \propto 1/T$. The behavior versus electronic density is compatible with a $1/g$ dependence of magnetopolarizability.

The magnetic response has been measured on the very same array of rings. The rings exhibits a signal consistent with *diamagnetic* average persistent currents of amplitude $|I_0|=0.25\pm0.1$ nA. Because the measurements are done on the same rings it is possible to compare the electric and the magnetic signal. The experimental ratio between the frequency shift due to the electric or magnetic response is around 10, a value consistent with theoretical expectations taking into account the electric and magnetic coupling coefficient (Appendixes A and B) and the ratio between the typical matrix element of the screened potential and the current operator, which leads to[18]

$$\frac{\delta_\Phi \chi}{\delta_\Phi \alpha/\epsilon_0}\approx(Z_0G_D)^2\approx\alpha^2g^2, \tag{31}$$

with $Z_0=\sqrt{\mu_0/\epsilon_0}=377\ \Omega$ the vacuum impedance, $G_D=ge^2/h$ the Drude conductance, and $\alpha\approx1/137$ the fine-structure constant. We have thus shown that the mesoscopic electromagnetic response of GaAs rings is dominated by the flux-dependent polarizability instead of orbital magnetism. This would not be the case in metallic rings, where, due to the very short screening length, the mesoscopic electric response is negligible. The low-field diamagnetic sign of the orbital magnetism needs further investigation both on the experimental and theoretical sides.

ACKNOWLEDGMENTS

We thank B. Etienne for the fabrication of the heterojunction. We acknowledge fruitful discussions with L.P. Lévy, Ya.M. Blanter, S. Guéron and G. Montambaux, and the technical help of M. Nardone and P. Demianozuck.

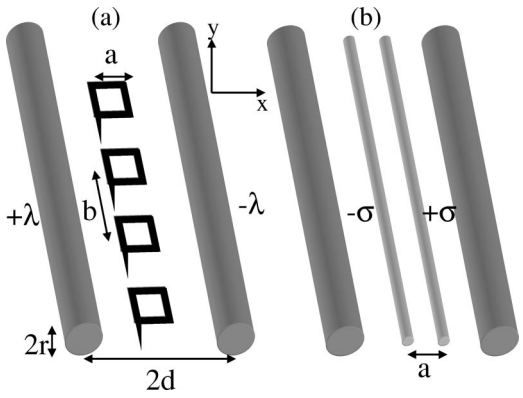

FIG. 20. (a) Schematic picture of the rings coupled to the capacitance. (b) Modelization used for the estimation of the electric coupling coefficient. The linear charge σ is determined by the polarizability of the rings and the electric field generated by the capacitance at the ring position.

APPENDIX A: EVALUATION OF THE MAGNETIC COUPLING

In this appendix we evaluate the magnetic coupling of one square ring with the resonator in the configuration of the experiment. The inductance $\mathcal{L}$ is modeled by two cylindrical wires separated by a distance of $2d$ [see Fig. 20(a)]. A ring is submitted to the magnetic field of those wires. Let us first evaluate the mutual inductance $\mathcal{M}$ between the ring and the resonator. Using Ampere's theorem the magnetic field generated by a current I in the the inductance is easily calculated. The flux of this magnetic field through a ring of size a located at the (0,0) point is then

$$\Phi=\mathcal{M}I=\frac{\mu_0 a}{\pi}\ln\left(\frac{2d+a}{2d-a}\right)I. \tag{A1}$$

If the ring is located at a point (x,y), $\mathcal{M}$ reads

$$\mathcal{M}=\frac{\mu_0 a}{4\pi}\ln\frac{[(x+d+a/2)^2+y^2][(x-d-a/2)^2+y^2]}{[(x+d-a/2)^2+y^2][(x-d+a/2)^2+y^2]}. \tag{A2}$$

The ring submitted to a magnetic field B acts as a magnetic dipole $m=\chi B/\mu_0$. This dipole is equivalent to the ring with a current m/a^2, so that the flux in the inductance is now $\Phi=(\mathcal{L}+\mathcal{M}^2\chi/a^4)I$. We deduce from these results that $k_m=\mathcal{M}^2/(\mu_0 a^4\mathcal{L})$ with $\mathcal{L}$ the inductance of the meander line. From the resonance frequency and the calculation of the capacitance we deduce $\mathcal{L}=0.05\ \mu$H. The rings are not perfectly well coupled to the inductance so that they are not all located at $x=0$. Moreover, because of the Mylar sheet inserted between the rings and the resonator, the rings are not in the plane of the resonator. To take this into account the inductance is averaged over the x position of the rings and $1.5\ \mu\text{m}<y<2.5\ \mu$m. Within these approximations, $k_m=1.3\times10^{11}\pm0.5\times10^{11}\ \text{m}^{-3}$.

APPENDIX B: EVALUATION OF THE ELECTRIC COUPLING

In this appendix we evaluate the electric coupling coefficient k of one ring with the capacitance $\mathcal{C}$ of the resonator. The capacitance is modeled by two cylindrical wires of radius r and separated by a distance $2d$, one wire with a linear charge of λ and the other one $-\lambda$. The electric field outside the wires is the one generated by two linear of lineic charge λ and $-\lambda$ separated by a distance $2d_1$ determined by $d_1 = \sqrt{d^2-r^2}$.[45] In our case $\mathcal{C}=10$ pF. Using the Gauss theorem we can easily calculate the electric field in the plane of the rings in every point (x,y) outside the wires:

$$E(x,y)=\frac{\lambda}{2\pi\epsilon_0}\left(\frac{x+d_1}{(x+d_1)^2+y^2}-\frac{x-d_1}{(x-d_1)^2+y^2}\right). \tag{B1}$$

A ring submitted to this field generates an electric dipole $P=\alpha E$ with α the polarizability of one ring, so that the rings submitted to electric field act as an ensemble of dipole. We model them by two line of linear charge σ and $-\sigma$ separated by a distance a, and such that $\sigma b=\alpha E/a$ (see Fig. 20). Note that to do so the electric field has to be constant on the scale of the rings: this is roughly the case. Evaluating the potential δV created by these two wires between each side of the capacitance, and using the relation $\delta V=-V\delta\mathcal{C}/\mathcal{C}$, we have for rings located at (x,y)

$$\frac{\delta\mathcal{C}}{\mathcal{C}}=\frac{\sigma}{2\lambda}\,\frac{\ln\dfrac{[(d-r-x-a/2)^2+y^2][(d-r+x-a/2)^2+y^2]}{[(d-r-x+a/2)^2+y^2][(d-r+x+a/2)^2+y^2]}}{\ln(d_1^2/r^2)}. \tag{B2}$$

To have the capacitance shift induced by one ring we have to divide the previous result by the number of rings $N=l/b$ with l the length of the capacitance. Moreover, as the rings are embedded in GaAs-$Al_xGa_{1-x}As$ we have to divide our result by the dielectric constant of the substrate $\epsilon_r=12.85$. We can now evaluate the electric coupling coefficient k_e defined by $\delta\mathcal{C}/\mathcal{C}=Nk_e\alpha$ by averaging over the x position of the rings and considering that the rings are located between 1.5 μm and 2.5 μm in the y direction from the resonator. Within these approximations $\epsilon_0\epsilon_r k_e=8\times10^{10}\pm3.4\times10^{10}$ m^{-3}. Note that the previous result is very close to the value of the magnetic coupling coefficient k_m.

APPENDIX C: MAGNETOPOLARIZABILITY FOR A QUASI-1D RING

In this appendix we evaluate the magnetopolarizability given by formula (13) for a quasi-1D ring. The diffusion propagator at frequency ω is given by

$$\Pi_D(\mathbf{r},\mathbf{r}',\omega)=\frac{\Delta S}{\pi}\sum_n\frac{\psi_n^*(\mathbf{r})\psi_n(\mathbf{r}')}{-i\omega+E_n} \tag{C1}$$

S and Δ are respectively the surface of the ring and the mean level spacing. E_n and ψ_n are the eigenvalues and eigenvectors of the diffusion equation

$$-\hbar D\Delta_r\psi_n(\mathbf{r})=E_n\psi_n(\mathbf{r}). \tag{C2}$$

We consider a 2D ring of perimeter L, radius R, and width W, with $W\ll L$. In this case the solutions of the diffusion equation are

$$\psi_{m,n}(x,y)=\sqrt{\frac{2}{LW}}\cos\left(\pi m\frac{y}{W}\right)\exp\left(i2\pi n\frac{x}{L}\right) \tag{C3}$$

with $m\in\mathbb{N}^*$ and $n\in\mathbb{Z}$. The modes corresponding to $m=0$ are given by

$$\psi_{m=0,n}(x,y)=\sqrt{\frac{1}{LW}}\exp\left(i2\pi n\frac{x}{L}\right). \tag{C4}$$

x is the coordinate along the ring, and y the radial coordinate. In our description the ring corresponds to $y\in[0,W]$. We consider the reflecting border in the y direction.The corresponding eigenvalue is

$$E_{m,n}=E_c\left[2\pi n^2+m^2\frac{\pi}{2}\left(\frac{L}{W}\right)^2\right]. \tag{C5}$$

$E_c=hD/L^2$ is the Thouless energy. The mean charge density (average over the width of the ring) in the ring submitted to an electric field E is

$$\rho(x=R\cos\theta,y)=\frac{\epsilon_0\pi RE}{W\ln(R/W)}\cos\theta. \tag{C6}$$

Note that using this density we recover the classical result for a quasi-1D ring $\alpha_{1D}=\epsilon_0\pi^2R^3/\ln(R/W)$. In the Thomas-Fermi approximation we deduce the mean screened potential

$$F(x=R\cos\theta,y)=\frac{R\lambda_s E}{2W\ln(R/W)}\cos\theta. \tag{C7}$$

Using this relation and the formula for the diffuson one can do the calculation analytically. Because of the form of F only the mode $(m=0,\ n=1)$ remains and leads to

$$\frac{\delta_\Phi\alpha'}{\alpha_{1D}}=\epsilon_r f\left(\frac{L}{W}\right)\frac{\lambda_s}{W}\frac{\Delta}{E_c}, \tag{C8}$$

with $f(x)=1/(4\pi^2\ln x/2\pi)$.

[1] See, e.g., *Mesoscopic Phenomena in Solids*, edited by B. L. Altshuler, P. A. Lee, and R. A. Webb (Elsevier, Amsterdam, 1991); Y. Imry, *Introduction to Mesoscopic Physics* (Oxford University Press, New York, 1997).
[2] S. Washburn and R. A. Webb, Adv. Phys. **35**, 375 (1986).
[3] D. Yu. Sharvin and Yu. V. Sharvin, Pis'ma Zh. Éksp. Teor. Fiz. **34**, 285 (1981) [JETP Lett. **34**, 272 (1981)].
[4] A. G. Aronov and Yu. V. Sharvin, Rev. Mod. Phys. **59**, 755 (1987).
[5] A. M. Chang, H. U. Baranger, L. N. Pfeiffer, and K. W. West, Phys. Rev. Lett. **73**, 2111 (1994).
[6] Y. Lee, G. Faini, and D. Mailly, Phys. Rev. B **56**, 9805 (1997).
[7] B. Reulet, M. Ramin, H. Bouchiat, and D. Mailly, Phys. Rev. Lett. **75**, 124 (1995).
[8] M. Büttiker, Y. Imry, and R. Landauer, Phys. Rev. **96**, 365 (1983).
[9] For a review see, e.g., U. Eckern and P. Schwab, Adv. Phys. **44**, 387 (1995).
[10] V. Chandrasekhar *et al.*, Phys. Rev. Lett. **67**, 3578 (1991).
[11] E. M. Q. Jariwala, P. Mohanty, M. B. Ketchen, and R. A. Webb, Phys. Rev. Lett. **86**, 1594 (2001).
[12] D. Mailly, C. Chapelier, and A. Benoit, Phys. Rev. Lett. **70**, 2020 (1993).
[13] L. P. Lévy, G. Dolan, J. Dunsmuir, and H. Bouchiat, Phys. Rev. Lett. **64**, 2074 (1990).
[14] S. Strässler, M. J. Rice, and P. Wyder, Phys. Rev. B **6**, 2575 (1972); M. J. Rice, W. R. Schneider, and S. Strässler, *ibid.* **8**, 474 (1973).
[15] K. B. Efetov, Phys. Rev. Lett. **76**, 1908 (1996).
[16] Y. Noat, B. Reulet, and H. Bouchiat, Europhys. Lett. **36**, 701 (1996).
[17] Ya. M. Blanter and A. D. Mirlin, Phys. Rev. B **57**, 4566 (1998).
[18] Y. Noat, B. Reulet, H. Bouchiat, and D. Mailly, Superlattices Microstruct. **23**, 621 (1998).
[19] R. Deblock, Y. Noat, H Bouchiat, B. Reulet, and D. Mailly, Phys. Rev. Lett. **84**, 5379 (2000).
[20] T. Sajoto, Y. W. Suen, L. W. Engel, M. B. Santos, and M. Shayegan, Phys. Rev. B **41(12)**, 8449 (1990).
[21] T. Ando, A. Fowler, and F. Stern, Rev. Mod. Phys. **54**, 437 (1982).
[22] These values are deduced from weak localization measurements on connected wires etched in the same heterojunction than the rings.
[23] J. P. Carini, K. A. Muttalib, and S. R. Nagel, Phys. Rev. Lett. **53**, 102 (1984); A. Kamenev and Y. Gefen, Phys. Rev. B **49**, 14 474 (1994).
[24] L. P. Gor'kov and G. M. Eliashberg, Zh. Éksp. Teor. Phys. **48**, 1407 (1965) [Sov. Phys. JETP **21**, 940 (1965)].
[25] M. Büttiker, Phys. Scr. **54**, 104 (1994); M. Büttiker and C. A. Stafford, Phys. Rev. Lett. **76**, 495 (1996).
[26] Y. Noat, R. Deblock, B. Reulet, and H. Bouchiat, cond-mat/0107408 (unpublished).
[27] Ya. M. Blanter and A. D. Mirlin, Phys. Rev. B **63**, 113315 (2001).
[28] Ya. M. Blanter and A. D. Mirlin, Phys. Rev. B **53**, 12 601 (1996).
[29] A. D. Mirlin, Phys. Rep. **326**, 259 (2000).
[30] M. L. Mehta, *Random Matrices and the Statistical Theory of Energy Levels* (Academic, New York, 1967).
[31] Ya. M. Blanter, Phys. Rev. B **54**, 12 807 (1996).
[32] B. Reulet, H. Bouchiat, and D. Mailly, Europhys. Lett. **31**, 305 (1995).
[33] B. L. Altshuler and A. G. Aronov, in *Electron-Electron Interactions in Disordered Systems* (North Holland, Amsterdam, 1985).
[34] U. Sivan, Y. Imry, and A. G. Aronov, Europhys. Lett. **28**, 115 (1994).
[35] Y. Noat, H. Bouchiat, B. Reulet, and D. Mailly, Phys. Rev. Lett. **80**, 4955 (1998).
[36] N. Trivedi and D. A. Browne, Phys. Rev. B **38**, 9581 (1988).
[37] A. Kamenev and Y. Gefen, Phys. Rev. Lett. **70**, 1976 (1993).
[38] A. Kamenev, B. Reulet, H. Bouchiat, and Y. Gefen, Europhys. Lett. **28**, 391 (1994).
[39] U. Sivan and Y. Imry, Phys. Rev. B **35**, 6074 (1987).
[40] B. Reulet and H. Bouchiat, Phys. Rev. B **50**, 2259 (1994).
[41] V. Ambegaokar and U. Eckern, Phys. Rev. Lett. **65**, 381 (1990).
[42] B. L. Altshuler, Y. Gefen, and Y. Imry, Phys. Rev. Lett. **66**, 88 (1991).
[43] V. E. Kravtsov and V. I. Yudson, Phys. Rev. Lett. **70**, 210 (1993).
[44] V. E. Kravtsov and B. L. Altshuler, Phys. Rev. Lett. **84**, 3394 (2000).
[45] L. D. Landau and E. M. Lifchitz, *Electrodynamics of Continuous Media* (MIR, Moscow, 1969).